OPTICA

Noise-resistant quantum communications using hyperentanglement

Jin-Hun Kim,[1] Yosep Kim,[1] Dong-Gil Im,[1] Chung-Hyun Lee,[1] Jin-Woo Chae,[1] Giuliano Scarcelli,[2,3] and Yoon-Ho Kim[1,4]

[1]Department of Physics, Pohang University of Science and Technology (POSTECH), Pohang 37673, Republic of Korea
[2]Fischell Department of Bioengineering, University of Maryland, College Park, Maryland 20742, USA
[3]e-mail: scarc@umd.edu
[4]e-mail: yoonho72@gmail.com

Received 1 September 2021; revised 5 November 2021; accepted 9 November 2021; published 1 December 2021

Quantum information protocols are being deployed in increasingly practical scenarios, via optical fibers or free space, alongside classical communications channels. However, entanglement, the most critical resource to deploy to the communicating parties, is also the most fragile to the noise-induced degradations. Here we show that polarization-frequency hyperentanglement of photons can be effectively employed to enable noise-resistant distribution of polarization entanglement through noisy quantum channels. In particular, we demonstrate that our hyperentanglement-based scheme results in an orders-of-magnitude increase in the SNR for distribution of polarization-entangled qubit pairs, enabling quantum communications even in the presence of strong noise that would otherwise preclude quantum operations due to noise-induced entanglement sudden death. While recent years have witnessed tremendous interest and progress in long-distance quantum communications, previous attempts to deal with the noise have mostly been focused on passive noise suppression in quantum channels. Here, via the use of hyperentangled degrees of freedom, we pave the way toward a universally adoptable strategy to enable entanglement-based quantum communications via strongly noisy quantum channels.

https://doi.org/10.1364/OPTICA.442240

1. INTRODUCTION

Distribution of quantum entanglement to two or more distant parties is the essential operation that powers nearly all quantum information protocols, such as quantum key distribution [1–3], quantum teleportation [4–7], quantum secret sharing [8,9], quantum secure direct communications [10,11], deterministic secure quantum communications [12–14], and connecting quantum processing nodes [15,16]. For the practical deployment of long-distance quantum communications protocols, distribution of entanglement through noisy quantum channels remains a critical unsolved gap [17,18]. Indeed, the presence of noise within the quantum transmission channels, via free space or optical fibers, is nearly unavoidable because it can come from stray light, the cross talk of co-propagating signals, or can be generated by linear and nonlinear effects in the transmission medium itself [19,20]. The effects of noise to a quantum state can be described fully by a few quantum error models [21]; for instance, after being transmitted through quantum channels with depolarizing noise, a perfectly prepared entangled state, $|\phi^{(+)}\rangle = (|00\rangle + |11\rangle)/\sqrt{2}$, quickly degrades to a partially mixed state, $\rho = (1-p)|\phi^{(+)}\rangle\langle\phi^{(+)}| + p\mathbb{1}/4$, where $\mathbb{1}$ is the identity operator. Quantum operations cease to be possible at $p > 2/3$ because there would be no entanglement shared between two distant quantum nodes.

Given the importance of entanglement distribution for quantum information, a substantial effort for noise suppression within transmission channels has led to impressive demonstrations of long-distance quantum communications in recent years. Noise suppression is, however, a practical strategy limited to specific experimental conditions that may fall short of enabling the widespread implementation of quantum protocols. In terms of robustness to noise, entanglement of high dimensional quantum states (qudits) may offer an advantage over entangled qubits [22,23], but it depends heavily on the noise and channel characteristics as well as the detection modality [24]. Moreover, the actual viability of such protocols is not clear, given the added experimental and theoretical complexities of qudits and the fact that the majority of quantum information protocols are qubit-based. In this paper, we address, for what we believe is the first time, the fundamental fragility of entanglement distribution in qubit-based quantum communications systems by enhancing their ability to withstand quantum state degradation within noisy channels in a practically deployable fashion via hyperentanglement.

Hyperentanglement refers to a multipartite quantum state that is simultaneously entangled in two or more separate degrees of freedom, e.g., position–momentum, energy–time, polarization, orbital angular momentum, and time bin [25–27], and it has been used for demonstrating certain quantum information protocols such as high-capacity encoding [28] and superdense

teleportation [29,30]. Here, in contrast to previous utilizations of hyperentanglement, our scheme does not require modification of the intrinsic quantum communications protocol under exam. Indeed, our noise-resistant protocol can be directly applicable to all the qubit-based communications protocols. Instead, we take advantage of the fundamental property of hyperentanglement; i.e., the additional quantum correlation in a different Hilbert space to efficiently discriminate the signal photons from noise photons coming from other sources, resulting in a several orders of magnitude enhancement of the SNR. We demonstrate that our hyperentanglement-based protocol enables extremely robust distribution of polarization-entangled photons even in the presence of strong noise that would otherwise preclude quantum operations due to noise-induced entanglement sudden death. Being rooted in the inherent essence of hyperentanglement, the strategy we report here is generally applicable to a wide-ranging set of quantum communications protocols under current development with nearly no modifications.

2. RESULTS AND DISCUSSION

A conceptual scheme of the protocol is shown in Fig. 1(a). A pair of photons hyperentangled in polarization and frequency-time degrees of freedom is prepared and sent to two distant parties, Alice and Bob, via optical fibers where white noise is purposefully introduced to simulate noisy quantum channels. Incidentally, spontaneous parametric down-conversion (SPDC), the workhorse of photonic entanglement, can naturally produce two-photon states hyperentangled in polarization and frequency-time. The polarization degree of freedom constitutes the qubit, and the goal of the protocol is to distribute a pair of entangled qubits to Alice and Bob even via highly noisy quantum channels while maintaining a high SNR. To do so, we use the frequency-time entanglement of the photon pair [31–34], simultaneously present with the polarization entanglement. Note that, in a traditional protocol without using hyperentanglement, the detection module cannot distinguish the signal-entangled photons from the noise photons; hence, at a constant signal, the SNR degrades with the number of noise photons. In our scheme, before being detected, the two photons go through dispersive stages, acquiring chirp and anti-chirp, respectively, and the frequency-anticorrelation property of the SPDC photons makes possible the lossless conversion of the correlated frequency bins to the correlated time bins via dispersive media, enabling frequency-selective detection of photons based on the time-of-arrival measurements [35–37]. The pair photons that are anti-correlated in frequency will result in equal time coincidence clicks, while the noise photons with no frequency relation will elicit clicks at random time differences. To better visualize the noise-resistant property provided by the protocol, we divide detection in N frequency bins per detection station and thus imagine the coincidence counting as an $N \times N$ matrix featuring all possible frequency-bin combinations. The polarization-entangled photons, further endowed with frequency-anticorrelation due to hyperentanglement, will spread along the 1D diagonal of the matrix, while the noise photons will evenly spread across the whole 2D plane, as shown in Fig. 1(b). In other words, while the signal remains constant because it is fully captured in the diagonal elements, the noise is randomly and uniformly distributed in the 2D plane; hence, reduced by N/N^2. Thus, frequency-resolved detection via gated coincidence measurement enables effective rejection

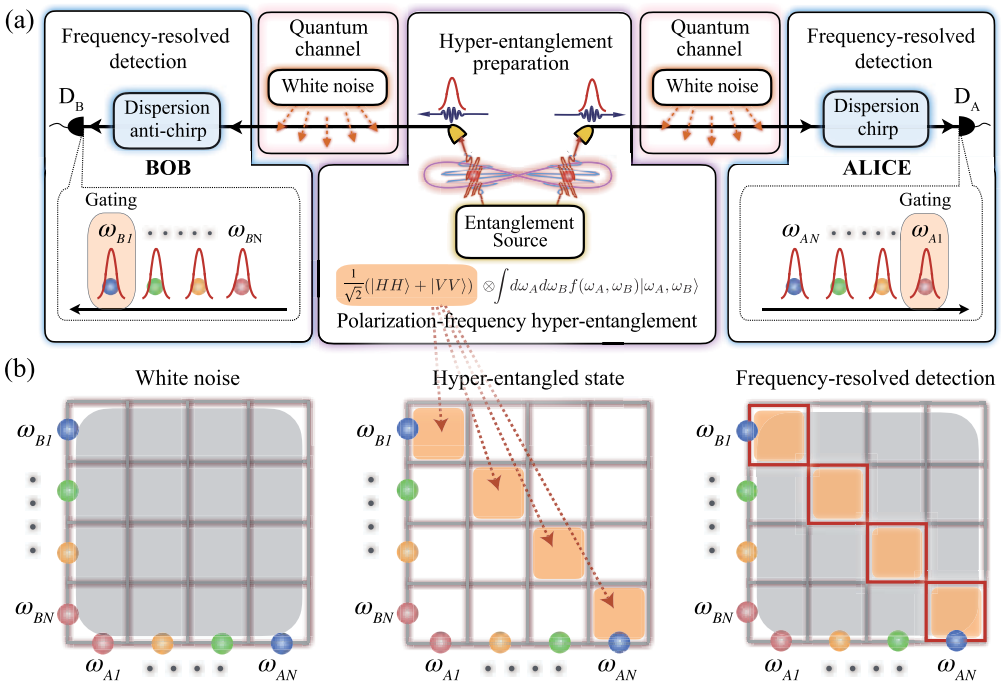

Fig. 1. (a) Conceptual schematic of noise-resistant quantum communications using polarization-frequency hyperentanglement. To distribute polarization entanglement to Alice and Bob through noisy quantum channels, frequency-time entanglement of the photons is used. The frequency-anticorrelation property of the photons makes possible the lossless conversion of the correlated frequency bins to the correlated time bins via dispersive media. Gated coincidence detection effectively performs measurement of correlated frequency bins. (b) Due to the frequency-anticorrelation nature of the photon pairs, the correlated frequency bins are anti-diagonally distributed, while the white noise from the quantum channels is not. Each correlated frequency bin represents a probability amplitude of a polarization-entangled photon pair. Frequency-resolved detection via gated coincidence measurement enables effective rejection of white noise, making possible noise-resistant quantum communications.

of all off-diagonal white noise in the matrix and, therefore, compared to ordinary quantum communications protocols relying on direct distribution of polarization entanglement, our protocol relying on polarization/frequency hyperentanglement gives rise to an N scaling advantage in SNR, making possible noise-resistant quantum communications. We first present the theoretical and numerical analysis of our protocol under realistic scenarios. We then describe the experimental implementation of the protocol, demonstrating the SNR improvement as well as entanglement distribution in the presence of strong noise.

The effects of the quantum noise to a pure maximally entangled state can be described by mixing the entangled state with a white noise state. As we consider the polarization-frequency hyperentangled state, the noisy polarization-frequency hyperentangled quantum state ρ_h may be described as

$$\rho_h = (1-p)|\phi^{(+)}\rangle\langle\phi^{(+)}| \otimes |\psi\rangle\langle\psi| + \frac{p}{4N^2}\mathbb{1}_{\text{pol}} \otimes \mathbb{1}_{\text{freq}}, \quad (1)$$

where p $(0 \le p \le 1)$ is the noise portion, $|\phi^{(+)}\rangle = \frac{1}{\sqrt{2}}(|HH\rangle + |VV\rangle)$, and $|\psi\rangle = \sum_{n=1}^{N} \frac{1}{\sqrt{N}}|n\rangle_1|n\rangle_2$ is the N-dimensional frequency entangled state. The identity operators $\mathbb{1}_{\text{pol}}$ and $\mathbb{1}_{\text{freq}}$ denote, respectively, the white noise states in the polarization and in the frequency degrees of freedom. Here, $4N^2$ represents the dimensional normalization for the white noise term. From Eq. (1), we first define the critical noise portion p_c at which the two-qubit state has no polarization entanglement and, by using the separability criterion for a density matrix [38,39], it is found to be $p_c = 2N/(1+2N)$. Note that if $p_c < 1$, the phenomenon is known as entanglement sudden death [40–44]. As the critical noise portion approaches one with a large N, the distribution of polarization entanglement becomes more robust to noise. Additionally, for the noisy entangled state in Eq. (1), the SNR is found to be

$$\text{SNR} = 2N(1-p)/p. \quad (2)$$

For more details, see Appendices A, B, and C. Note that at $p = p_c$, SNR becomes unity regardless of the dimension N. The noisy entangled state in Eq. (1) has nonzero entanglement if the measured SNR value exceeds one.

In our protocol, the SPDC photons are frequency-binned into N channels such that, for each channel, the channel efficiency (including the overall quantum channel transmission efficiency α_{ch} and the detector efficiency α_{d}) is $\alpha = \alpha_{\text{ch}}\alpha_{\text{d}}$, the dark count probability (per gate pulse) of a detector is d, and the detection probability (per gate pulse) of the background noise is b. If the average number of SPDC photon pairs per pulse is μ, the expression for the SNR is given as

$$\text{SNR} = \frac{\mu\alpha^2}{2N\left(\frac{\mu}{2N}\alpha + d + \frac{b}{2N}\right)^2}, \quad (3)$$

where we have assumed for simplicity that all N channels have identical properties (see Appendices A, B, and C for details). The results of the numerical simulation are shown in Fig. 2. As the frequency-resolved detection for the N correlated frequency bins is made possible by converting them into N correlated time bins, a detector having a faster rise time would enable tighter frequency-resolved detection. For the simulation, we assumed a rather weak SPDC process, $\mu = 0.02$, and the overall quantum channel efficiency of $\alpha_{\text{ch}} = 0.5$ for each photon. Considering the typical parameters of an InGaAs detector ($d = 6 \times 10^{-6}$ and $\alpha_{\text{d}} = 0.15$) and an SNSPD ($d = 6 \times 10^{-8}$ and $\alpha_{\text{d}} = 0.8$) at the telecom wavelength, the numerical simulation of Eq. (3) shown in Fig. 2 confirms that the white noise subtraction becomes more prominent as N is increased. It is important to point out that SNRs reach different maximum values and decrease with increasing N due to the contributions of the dark counts, as shown in Fig. 2. Clearly, there is an optimum value of N that maximizes SNR for a given initial noise portion p_1 and the detector properties. The numerical simulation clearly demonstrates that, even for highly noisy quantum channels represented by a large initial noise portion p_1, high SNR entanglement distribution is possible by choosing a suitable correlated time-bin division N. In particular, in Fig. 2, we have demonstrated that, showing up to three orders of magnitude SNR improvement for traditional InGaAs detectors and up to nearly six orders of magnitude SNR improvement for SNSPDs.

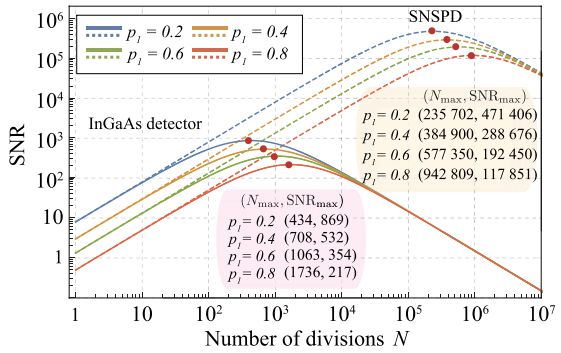

Fig. 2. SNR for entanglement distribution via noisy quantum channels. Here, we have assumed $\mu = 0.02$, $\alpha_{\text{ch}} = 0.5$, and typical parameters of an InGaAs detector ($d = 6 \times 10^{-6}$ and $\alpha_{\text{d}} = 0.15$) and SNSPD ($d = 6 \times 10^{-8}$ and $\alpha_{\text{d}} = 0.8$). Due to the contributions of the dark counts, SNR reaches a maximum value and decreases with increasing N. Even for highly noisy quantum channels (i.e., a large initial noise portion p_1), high SNR entanglement distribution is possible by choosing a suitable correlated time-bin division N.

We now describe the experimental demonstration of the protocol to confirm the SNR improvement in quantum communications, even in the presence of strong noise that would otherwise cause entanglement sudden death. The schematic of the experiment, based on a fiber-optic setup, is shown in Fig. 3. To prepare polarization-frequency hyperentanglement of two photons in telecom wavelength, we use the type-0 SPDC process in a PPLN crystal pumped by the second harmonic of a picosecond mode-locked fiber laser. While frequency entanglement of the photon pair is naturally provided by the SPDC process, to prepare the polarization-entangled state, we make use of an unbalanced Michelson interferometer (UMI) for the pump pulse and a phase-stabilized unbalanced polarization Mach–Zehnder interferometer for the SPDC photons [45,46]. For more details, see Appendices A, B, and C. The polarization-frequency hyperentangled state of the photon pair is then given as

$$\frac{1}{\sqrt{2}}(|HH\rangle + |VV\rangle) \otimes \int d\omega_1 d\omega_2 f(\omega_1, \omega_2)|\omega_1, \omega_2\rangle, \quad (4)$$

where $f(\omega_1, \omega_2)$ is the joint spectral amplitude of the two-photon state, exhibiting frequency anti-correlation between the two photons. The full spectral bandwidth $|f(\omega_1, \omega_2)|^2$ of the SPDC photons is roughly 80 nm at FWHM centered at 1552.52 nm. In our experiment, we make use of roughly 10 nm flap-top regions

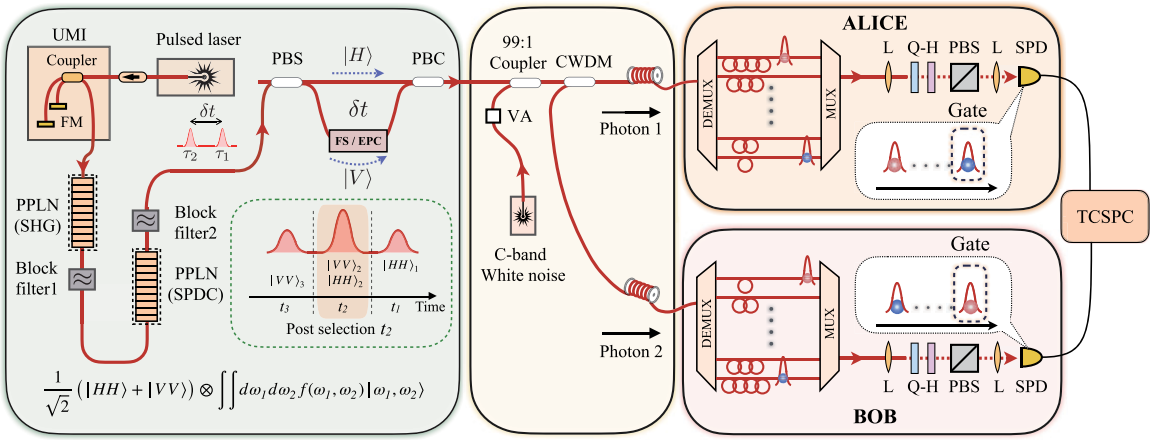

Fig. 3. Experimental setup for noise-resistant polarization-entanglement distribution using hyperentanglement. Second-harmonic of a pulsed laser ($\lambda_p = 1{,}552.52$ nm and $\delta\lambda_p = 0.15$ nm) produces a pair of frequency-anticorrelated entangled photons via the type-0 SPDC process in a PPLN crystal. Polarization entanglement is generated by quantum interference at the unbalanced Mach–Zehnder interferometer constructed with PBS and PBC. The spectral properties of the photons are $\lambda_1 = 1{,}545.32$ nm $\delta\lambda = 9.56$ nm for photon 1 (to Alice) and $\lambda_2 = 1{,}559.79$ nm $\delta\lambda_2 = 9.74$ nm for photon 2 (to Bob). The white noise is sourced from a C-band laser and is bandwidth matched to photon 1 and photon 2. Conversion from the frequency-bin to the time-bin modes is accomplished with a pair of DWDM DEMUX and a MUX connected by optical fibers of different lengths. UMI, unbalanced Michelson interferometer; PPLN, periodically poled lithium niobate; SHG, second-harmonic generation; SPDC, spontaneous parametric downconversion; PC, polarization controller; FS: fiber stretcher, EPS, electronic polarization controller; PBS, polarizing beam splitter; PBC, polarizing beam combiner; CWDM, coarse wavelength division multiplexing; L, lens, HWP, half-wave plate; and SPD, single photon detector.

of the spectral bandwidth for the frequency-entangled photons: For photon 1, the central wavelength is $\lambda_1 = 1{,}545.32$ nm and the bandwidth is $\delta\lambda_1 = 9.56$ nm; for photon 2, the central wavelength is $\lambda_2 = 1{,}559.79$ nm and the bandwidth is $\delta\lambda_2 = 9.74$ nm. To test the noise-resistant feature of the protocol, it is necessary to introduce white noise to the entangled state so that the state in Eq. (1) can be prepared. In our experiment, we use a broadband telecom C-band light source, which is bandwidth-matched to those of photon 1 and photon 2. The attenuated white noise is then introduced to the fiber optic channel to Alice and Bob via a 99:1 coupler. The noise portion in Eq. (1) can be measured in the experiment as the ratio of the rate of noise counts and the rate of total counts at a detector.

At the heart of the protocol is to discretize the correlated spectra of the polarization-frequency hyperentangled photon pairs and to deterministically map the correlated frequency bin measurement to the correlated time-bin measurement. If photon 1 and photon 2 spectra are each discretized into N bins, the quantum state in Eq. (4) can be written as

$$\frac{1}{\sqrt{2}}(|HH\rangle + |VV\rangle) \otimes \sum_{n=1}^{N} \frac{1}{\sqrt{N}} |n\rangle_1 |n\rangle_2, \tag{5}$$

where N is the total number of frequency bins and $|n\rangle_1|n\rangle_2$ refers to the quantum state of the correlated frequency bin n for photon 1 and photon 2. Instead of using dispersive chirp and anti-chirp media, as shown in Fig. 1, for frequency-bin to time-bin mapping, in our experiment, we use readily available dense wavelength division multiplexing (DWDM) components in the telecom band. By using a demultiplexer (DEMUX), we divide the available single-photon spectra into up to six spectral channels, each with a FWHM bandwidth of 1.2 nm and channel spacing of 1.6 nm. The six DEMUX output channels are connected to optical fibers of different lengths and fiber polarization controllers. They are then recombined into a single-mode optical fiber by using a multiplexer (MUX). The frequency-bin separation of 1.6 nm thus is converted into the time-bin separation of 2.5 ns. Therefore, the joint spectrum analysis for photon 1 (spectral range between 1540.56 nm and 1550.12 nm) and photon 2 (spectral range between 1554.94 nm and 1564.67 nm), schematically shown in Fig. 1(b), can be performed in an experiment by measuring the 6×6 temporal correlation in the photons' arrival times at the InGaAs detectors using a coincidence counting device. Measurement on the polarization qubits can be done for each correlated time bin by using the standard polarization qubit analysis technique with a half-wave plate, a quarter-wave plate, and a polarizing beam splitter. For the correlated time-bin measurement, the detector's gate window is set at 1.5 ns. From the measurement, we reconstruct the 6×6 matrix that represents the frequency-bin entanglement and each correlated frequency bin represents a probability amplitude of a polarization-entangled photon pair. The 6×6 correlated frequency bins may be summed up to study the effect of more coarse frequency binning (e.g., 2×2 and 3×3) to the SNR.

The experimental SNR measurements for the polarization-entanglement distribution via noisy channels with hyperentangled discretized frequency-bin entanglement are shown in Fig. 4. For a given value of the noise portion p, we determine the experimental SNR values as a function of the number of frequency bins N. The noise portion p was determined from the ratio of the coincidence rate due to the noise only versus that due to both the signal and the noise. The SNR measurements were performed in the computational basis; i.e., $|HH\rangle$ and $|VV\rangle$. It is clear from Fig. 4(a) that our method improves the SNR quite significantly, even with a strong noise in the quantum channels, by introducing more frequency bins. In Figs. 4(b) and 4(c), the $N \times N$ measurement matrices are shown, revealing the effect of N binning detection (i.e., frequency binning) to the SNR for different values of the noise portion p. Note that for $N = 1$, the system is incapable of discriminating the signal and the noise photons; however, for $N = 2$, 3, and 6,

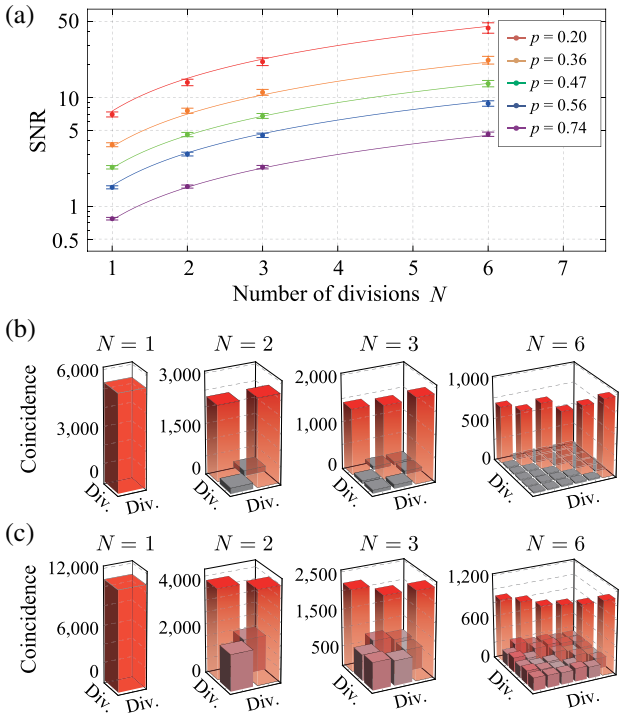

Fig. 4. SNR measurement data. (a) If the channel-induced noise portion p is high, tighter frequency-resolved detection (i.e., larger N), helps to increase SNR for polarization entanglement distribution. The error bars represent one standard deviation. The solid lines are due to the SNR equation in Eq. (2). The $N \times N$ measurement matrices are shown (b) for the noise portion $p = 0.2$ and (c) for the noise portion $p = 0.74$. Measurement outcomes due to polarization entangled photons are distributed only along the diagonal while those of the noise are distributed uniformly across the matrix. These figures clearly demonstrate the SNR improvement mechanism conceptually shown in Fig. 1(b). The data are accumulated for 90 s.

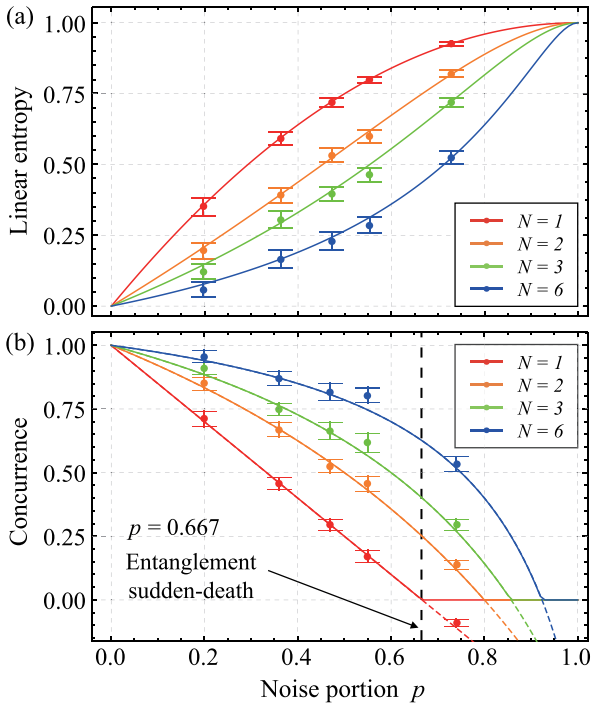

Fig. 5. Noise-resistant distribution of polarization entanglement using polarization-frequency hyperentanglement. Due to the N-binning detection (i.e., frequency binning), even for a large noise portion p, the distributed two-qubit state exhibits (a) significantly decreased linear entropy and (b) dramatically increased concurrence. Note that for $p \geq 0.667$, entanglement sudden death occurs as evidenced in the concurrence for $N = 1$ (i.e., $p_c = 2/3$ at $N = 1$). N binning detection, however, enables entanglement distribution even via highly noisy quantum channels. The solid lines represent the theoretical curves from the mixed two-qubit entanglement model. The error bars represent one standard deviation. The dashed lines and the data point below zero are due to $\lambda_1 - \lambda_2 - \lambda_3 - \lambda_4$.

the off-diagonal matrix elements are clearly identifiable as noise. Thus, the diagonal elements deal with significantly reduced noise. These data figures clearly demonstrate the SNR improvement mechanism conceptually shown in Fig. 1(b). Due to the frequency entanglement of the photon pair (simultaneously present with the polarization entanglement), the signal events are distributed along the diagonal of the $N \times N$ matrix, while the white noise is distributed evenly. Thus, by using a larger N, it becomes possible to significantly improve the SNR in distributing polarization entanglement, even with a strong noise in the quantum channel.

Next, we study the quality of polarization entanglement distributed to Alice and Bob via noisy quantum channels by varying the noise portion p and the number of frequency bins N. First, for a given value of the noise portion p, the two-qubit polarization state is fully characterized with quantum state tomography (QST) for $N = 1$, 2, 3 and 6. The two-qubit density matrix ρ obtained from QST is then used to evaluate the linear entropy $S_L = \frac{4}{3}(1 - \mathrm{Tr}[\rho^2])$ and the concurrence $C(\rho)$ of the two-qubit state [47]. The linear entropy for a two-qubit state ranges from zero for the case of a pure state and 1 for a maximally mixed state. The experimental results for the linear entropy are shown in Fig. 5(a). As the noise portion p is increased, it is clear that the two-qubit state becomes more mixed. However, as the number of frequency bins N is increased, the linear entropy is significantly reduced, implying that the two-qubit state shared between Alice and Bob becomes more pure. This is consistent with the data in Fig. 4(a), which shows an improvement of the SNR (i.e., an effective reduction of the noise), by using a larger N.

Figure 5(b) shows the concurrence $C(\rho)$ evaluated from the QST-reconstructed two-qubit density matrix ρ as the noise portion p is increased. Concurrence ranges from zero (i.e., no entanglement) to 1 (i.e., the Bell state) and is defined as $C(\rho) = \max(0, \lambda_1 - \lambda_2 - \lambda_3 - \lambda_4)$, where λ_i are the eigenvalues of the Hermitian matrix defined from ρ. Naturally, as p is increased, the concurrence of the two-qubit polarization state ρ is decreased. However, by using a larger N, we are able to dramatically increase concurrence between the two polarization qubits distributed to Alice and Bob. It is interesting to note that when $N = 1$ (the case of the ordinary detection method without relying on polarization-frequency hyperentaglement), entanglement sudden death occurs when $p = 0.667$. In Fig. 5(b), the dashed lines and the data point below the zero concurrence value are due to $\lambda_1 - \lambda_2 - \lambda_3 - \lambda_4$. Physically, it means that there is no entanglement. Remarkably, even in the case where noise is strong enough so that entanglement sudden death would make distribution of two-qubit polarization entanglement impossible, by using polarization-frequency hyperentanglement and frequency binning with a larger N, we are able to distribute nonzero entanglement to Alice and Bob.

3. CONCLUSION

Entanglement, the most critical resource in quantum information, is also the most fragile to the noise-induced degradations. In this work, we have proposed and demonstrated that hyperentangled degrees of freedom can be effectively employed to enable reliable entanglement distribution through noisy quantum channels. In particular, we have shown theoretically and experimentally that our protocol could result in an orders of magnitude increase in the SNR for polarization-entanglement distribution through highly noisy quantum transmission channels, enabling quantum communications even in the presence of strong noise that would otherwise preclude quantum operations due to noise-induced entanglement sudden death. Our protocol is qubit-based; hence, it does not require the complexity overhead of qudit-based protocols. The preparation of polarization-frequency hyperentanglement necessary for the protocol is simple using spontaneous parametric downconversion in a nonlinear crystal, and the components required for mapping correlated frequency bins to correlated time bins are readily available in the telecom band. Note that the noise-resistant feature may be significantly improved by optimizing the degree of energy-time correlation and using narrowband components for frequency binning. Moreover, being rooted in the inherent essence of hyperentanglement, the strategy we report here is generally applicable to a wide-ranging set of quantum communications protocols under current development with nearly no modifications. Finally, it is interesting to note that our scheme may be easily adopted for the distribution of entangled qudits by using energy-time hyperentanglement of the two-photon state, an approach that would greatly improve the noise-resistant feature of qudit entanglement far beyond what can be achieved naturally with entangled qudits alone. Therefore, we believe the scheme described in this work paves the way toward a universally adoptable practical strategy to withstand noise, by several orders of magnitude, in quantum communications via noisy channels.

APPENDIX A: POLARIZATION-FREQUENCY HYPERENTANGLEMENT

A picosecond mode-locked fiber laser (FPL-02CTT, Calmar Laser) operating at the center wavelength of 1552.52 nm (the FWHM bandwidth of 0.4 nm and the repetition rate of 18.02 MHz) is frequency doubled at the bulk type-0 PPLN crystal, which is 35 mm long and has the poling period of 19.3 μm. The pump pulse ($\lambda_p \approx 776.26$ nm) generates the broadband frequency-entangled 45° polarized SPDC photon pair $|DD\rangle$ centered at 1552 nm at the waveguide-type type-0 PPLN, which is 20 mm long and has the poling period of 17.0 μm. To prepare polarization-frequency hyperentanglement, as shown in Fig. 3, we make use of the time-bin entanglement generation scheme based on an unbalanced Michelson interferometer (UMI) for the pump pulse and a phase-stabilized unbalanced polarization Mach–Zehnder interferometer for the SPDC photons [45,46,48]. In the end, three two-photon amplitudes ($|HH\rangle$, $(|HH\rangle + |VV\rangle)/\sqrt{2}$, and $|VV\rangle$) are created in time, separated by 20.8 ns. The middle amplitude is post-selected to prepare the Bell state $(|HH\rangle + |VV\rangle)/\sqrt{2}$ in a single spatial mode. As photon 1 and photon 2 are chosen to have nondegenerate central wavelengths of $\lambda_1 = 1{,}545.32$ nm and $\lambda_2 = 1{,}559.79$ nm, respectively, they are eventually separated into two spatial modes by using a CWDM acting as a notch filter, which transmits photon 1 to Alice and reflects photon 2 to Bob. Alice and Bob therefore receive the polarization-frequency entangled photon pair in the state shown in Eq. (4).

APPENDIX B: INTERFEROMETERS

Two interferometers are used in the experiment: an unbalanced Michelson interferometer (UMI) for the pump and an unbalanced Mach-Zehnder interferometer (UMZI) for the SPDC photons. They are used, respectively, to introduce and to compensate for the time delay of 20.8 ns. The UMI consists of two Faraday mirrors for auto-compensating polarization mode dispersion, a variable delay line for fine-tuning the time delay, and a piezo-actuated fiber stretcher for precise phase control. The UMZI introduces the set time delay of 20.8 ns between $|H\rangle$ and $|V\rangle$ polarization modes by using a fiber optic polarizing beam splitter and a fiber optic polarizing beam combiner. The $|H\rangle$ path is implemented with a polarization-maintaining fiber while the $|V\rangle$ is implemented with a standard single-mode fiber, a variable delay line, a piezo-actuated fiber stretcher, and an electronically driven fiber polarization controller. To actively stabilize the interferometers, we use an auxiliary cw laser at 1553.33 nm whose coherence time is significantly larger than the time delay at the interferometers. Active phase stabilization of the interferometers is accomplished by monitoring the interference signals of the auxiliary cw laser and using them to feedback control the piezo-actuated fiber stretcher.

APPENDIX C: NOISY TWO-QUBIT STATES AND SNR

Noise in the quantum transmission channel degrades an initial pure polarization-frequency hyperentangled two-qubit state, resulting in a mixed state shown in Eq. (1). In our protocol, only the correlated frequency bins are relevant for the frequency degree of freedom; thus, Eq. (1) is simplified to $\rho_{\text{pol}} = \sum_{n=1}^{n=N} \langle nn|\rho_h|nn\rangle = \mathcal{A}\{(1-p)|\phi^{(+)}\rangle\langle\phi^{(+)}| + p\mathbb{1}_{\text{pol}}/4N\}$, where $\mathcal{A} = (1 + p(1/N - 1))^{-1}$ is the renormalization constant. The critical noise portion p_c, which is the maximum value of the noise portion p for the state to have nonzero entanglement, can be calculated using the positive partial transpose criterion; i.e., $(\mathbb{1} \otimes T)\rho_{\text{pol}} \geq 0$ [38,39]. For the minimum eigenvalue to be positive, $p_c = 2N/(1+2N)$. In addition, the two qubit state ρ_{pol} has the signal contribution equal to $\sum_i^{HH,VV} \langle i|\mathcal{A}(1-p)|\phi^{(+)}\rangle\langle\phi^{(+)}|i\rangle = \mathcal{A}(1-p)$. Similarly, the noise contribution is evaluated to be $\sum_i \langle i|p\mathbb{1}_{\text{pol}}/4N|i\rangle = \mathcal{A}p/2N$. Thus, we obtain the SNR expression in Eq. (2).

In our protocol, SNR is the ratio of the joint detection rate due to the two-qubit quantum state and the coincidence rate arising from the noise that cannot be removed from the correlated frequency bin detection. While the signal is only distributed along the diagonal in the correlated frequency bins, the noise is evenly distributed, see Fig. 1(b). Thus, although the correlated frequency bin detection removes all the off-diagonal noise contributions, the noise present in the diagonal terms would reduce SNR. The overall joint count rate can be expressed as

$$\sum_{x=1}^{2}\left(\sum_{j=1}^{N}\frac{\mu}{2N}\alpha_{1,x,j}\alpha_{2,x,j} + \sum_{j=1}^{N}\left(\frac{\mu}{2N}\alpha_{1,x,j} + d_{1,x,j} + \frac{b_1}{2N}\right)\left(\frac{\mu}{2N}\alpha_{2,x,j} + d_{2,x,j} + \frac{b_2}{2N}\right) + \sum_{i,j=1,i\neq j}^{N}\left(\frac{\mu}{2N}\alpha_{1,x,i} + d_{1,x,i} + \frac{b_1}{2N}\right)\left(\frac{\mu}{2N}\alpha_{2,x,j} + d_{2,x,j} + \frac{b_2}{2N}\right)\right),$$

where subscripts 1 and 2 refer to photon 1 and photon 2, x refers to the polarization qubit measurement basis, and i refers to the ith frequency bin. Here, the first term is the signal due to the two-qubit quantum state, the second term refers to noise in the diagonal bins, and the third term can be removed by the correlated frequency bin detection. The SNR thus can be written as the ratio of the first term and the second term. Assuming that all N channels have identical properties, we arrive at the SNR expression in Eq. (3). Note, however, that in our setup in Fig. 3 to prepare polarization entanglement we make use of the time bin post-selection scheme and this changes the count rate slightly, affecting the SNR expression. The revised SNR expression for our specific setup is given as $\frac{\mu\alpha^2}{8N}(\frac{\mu}{4N}\alpha + d + \frac{b}{2N})^{-2}$, which is slightly different from Eq. (3). The experimental SNR values in Fig. 4(a) have been evaluated with this form. Note that, if the polarization-frequency hyperentangled photons were generated directly from the nonlinear crystal, Eq. (3) would need to be used.

Funding. National Research Foundation of Korea (2019R1A2C3004812); ITRC support program (IITP-2021-2020-0-01606); National Science Foundation (1942003).

Acknowledgment. Authors Giuliano Scarcelli and and Yoon-Ho Kim designed the research. Author Jin-Hun Kim, with the help of authors Yosep Kim, Dong-Gil Im, Chung-Hyun Lee, and Jin-Woo Chae performed the experiment. All authors analyzed the data and discussed the results. Author Yoon-Ho Kim supervised the research. Authors Jin-Hun Kim, Giuliano Scarcelli, and Yoon-Ho Kim wrote the paper with input from all the authors.

Disclosures. The authors declare no conflicts of interest.

Data Availability. Data underlying the results presented in this paper are not publicly available at this time but may be obtained from the authors upon reasonable request.

REFERENCES

1. A. Ekert, "Quantum cryptography based on Bell's theorem," Phys. Rev. Lett. **67**, 661–663 (1991).
2. R. Ursin, F. Tiefenbacher, T. Schmitt-Manderbach, H. Weier, T. Scheidl, M. Lindenthal, B. Blauensteiner, T. Jennewein, J. Perdigues, P. Trojek, B. Ömer, M. Fürst, M. Meyenburg, J. Rarity, Z. Sodnik, C. Barbieri, H. Weinfurter, and A. Zeilinger, "Entanglement-based quantum communication over 144 km," Nat. Phys. **3**, 481–486 (2007).
3. J. Yin, Y.-H. Li, S.-K. Liao, *et al.*, "Entanglement-based secure quantum cryptography over 1120 kilometres," Nature **582**, 501–505 (2020).
4. D. Bouwmeester, J.-W. Pan, K. Mattle, M. Eibl, H. Weinfurter, and A. Zeilinger, "Experimental quantum teleportation," Nature **390**, 575–579 (1997).
5. D. Boschi, S. Branca, F. De Martini, L. Hardy, and S. Popescu, "Experimental realization of teleporting an unknown pure quantum state via dual classical and Einstein-Podolsky-Rosen channels," Phys. Rev. Lett. **80**, 1121–1125 (1998).
6. Y.-H. Kim, S. P. Kulik, and Y. Shih, "Quantum teleportation of a polarization state with a complete Bell state measurement," Phys. Rev. Lett. **86**, 1370–1373 (2001).
7. D.-G. Im, C.-H. Lee, Y. Kim, H. Nha, M. S. Kim, S.-W. Lee, and Y.-H. Kim, "Optimal teleportation via noisy quantum channels without additional qubit resources," npj Quantum Inf. **7**, 86 (2021).
8. M. Hillery, V. Buzek, and A. Berthiaume, "Quantum secret sharing," Phys. Rev. A **59**, 1829–1834 (1999).
9. S. Gaertner, C. Kurtsiefer, M. Bourennane, and H. Weinfurter, "Experimental demonstration of four-party quantum secret sharing," Phys. Rev. Lett. **98**, 020503 (2007).
10. G.-L. Long and X.-S. Liu, "Theoretically efficient high-capacity quantum-key-distribution scheme," Phys. Rev. A **65**, 032302 (2002).
11. Z. Qi, Y. Li, Y. Huang, J. Feng, Y. Zheng, and X. Chen, "A 15-user quantum secure direct communication network," Light Sci. Appl. **10**, 183 (2021).
12. X.-H. Li, F.-G. Deng, C.-Y. Li, Y.-J. Liang, P. Zhou, and H.-Y. Zhou, "Deterministic secure quantum communication without maximally entangled states," J. Korean Phys. Soc. **49**, 1354–1359 (2006).
13. D. Jiang, Y. Chen, X. Gu, L. Xie, and L. Chen, "Deterministic secure quantum communication using a single d-level system," Sci. Rep. **7**, 44934 (2017).
14. Y.-C. Jeong, S.-W. Ji, C. Hong, H.-S. Park, and J. Jang, "Deterministic secure quantum communication on the BB84 system," Entropy **22**, 1268 (2020).
15. D. Gottesman and I. L. Chuang, "Demonstrating the viability of universal quantum computation using teleportation and single-qubit operations," Nature **402**, 390–393 (1999).
16. E. Knill, R. Laflamme, and G. J. Milburn, "A scheme for efficient quantum computation with linear optics," Nature **409**, 46–52 (2001).
17. L.-M. Duan, M. D. Lukin, J. I. Cirac, and P. Zoller, "Long-distance quantum communication with atomic ensembles and linear optics," Nature **414**, 413–418 (2001).
18. H. J. Kimble, "The quantum internet," Nature **453**, 1023–1030 (2008).
19. L.-J. Wang, K.-H. Zou, W. Sun, Y. Mao, Y.-X. Zhu, H.-L. Yin, Q. Chen, Y. Zhao, F. Zhang, T.-Y. Chen, and J.-W. Pan, "Long-distance copropagation of quantum key distribution and terabit classical optical data channels," Phys. Rev. A **95**, 012301 (2017).
20. Y. Mao, B.-X. Wang, C. Zhao, G. Wang, R. Wang, H. Wang, F. Zhou, J. Nie, Q. Chen, Y. Zhao, Q. Zhang, J. Zhang, T.-Y. Chen, and J.-W. Pan, "Integrating quantum key distribution with classical communications in backbone fiber network," Opt. Express **26**, 6010–6020 (2018).
21. Y.-C. Jeong, J.-C. Lee, and Y.-H. Kim, "Experimental implementation of a fully controllable depolarizing quantum operation," Phys. Rev. A **87**, 014301 (2013).
22. D. Collins, N. Gisin, N. Linden, S. Massar, and S. Popescu, "Bell inequalities for arbitrarily high-dimensional systems," Phys. Rev. Lett. **88**, 040404 (2002).
23. S. Ecker, F. Bouchard, L. Bulla, F. Brandt, O. Kohout, F. Steinlechner, R. Fickler, M. Malik, Y. Guryanova, R. Ursin, and M. Huber, "Overcoming noise in entanglement distribution," Phys. Rev. X **9**, 041042 (2019).
24. F. Zhu, M. Tyler, N. H. Valencia, M. Malik, and J. Leach, "Is high-dimensional photonic entanglement robust to noise?" AVS Quantum Sci. **3**, 011401 (2021).
25. J. T. Barreiro, N. K. Langford, N. A. Peters, and P. G. Kwiat, "Generation of hyperentangled photon pairs," Phys. Rev. Lett. **95**, 260501 (2005).
26. T.-M. Zhao, Y. S. Ihn, and Y.-H. Kim, "Direct generation of narrow-band hyperentangled photons," Phys. Rev. Lett. **122**, 123607 (2019).
27. C. Wang, C.-H. Lee, Y. Kim, and Y.-H. Kim, "Generation of hyperentangled photons in a hot atomic vapor," Opt. Lett. **45**, 1802–1805 (2020).
28. J. T. Barreiro, T.-C. Wei, and P. G. Kwiat, "Beating the channel capacity limit for linear photonic superdense coding," Nat. Phys. **4**, 282–286 (2008).
29. T. M. Graham, H. J. Bernstein, T.-C. Wei, M. Junge, and P. G. Kwiat, "Superdense teleportation using hyperentangled photons," Nat. Commun. **6**, 7185 (2015).
30. B. P. Williams, R. J. Sadlier, and T. S. Humble, "Superdense coding over optical fiber links with complete Bell-state measurements," Phys. Rev. Lett. **118**, 050501 (2017).
31. Y.-H. Kim and W. P. Grice, "Measurement of the spectral properties of the two-photon state generated via type-II spontaneous parametric down-conversion," Opt. Lett. **30**, 908–910 (2005).
32. S.-Y. Baek and Y.-H. Kim, "Spectral properties of entangled photons generated via type-I frequency-nondegenerate spontaneous parametric down-conversion," Phys. Rev. A **80**, 033814 (2009).
33. Y.-W. Cho, K.-K. Park, J.-C. Lee, and Y.-H. Kim, "Engineering frequency-time quantum correlation of narrow-band biphotons from cold atoms," Phys. Rev. Lett. **113**, 063602 (2014).
34. K.-K. Park, J.-H. Kim, T.-M. Zhao, Y.-W. Cho, and Y.-H. Kim, "Measuring the frequency-time two-photon wavefunction of narrowband entangled photons from cold atoms via stimulated emission," Optica **4**, 1293–1297 (2017).
35. S.-Y. Baek, O. Kwon, and Y.-H. Kim, "Nonlocal dispersion control of a single-photon waveform," Phys. Rev. A **78**, 013816 (2008).
36. S.-Y. Baek, Y.-W. Cho, and Y.-H. Kim, "Nonlocal dispersion cancellation using entangled photons," Opt. Express **17**, 19241–19252 (2009).
37. A. O. C. Davis, P. M. Saulnier, M. Karpiński, and B. J. Smith, "Pulsed single-photon spectrometer by frequency-to-time mapping using chirped fiber Bragg gratings," Opt. Express **25**, 12804–12811 (2017).

38. A. Peres, "Separability criterion for density matrices," Phys. Rev. Lett. **77**, 1413–1415 (1996).
39. M. Horodecki, P. Horodecki, and R. Horodecki, "Separability of mixed states: necessary and sufficient conditions," Phys. Lett. A **223**, 1–8 (1996).
40. M. P. Almeida, F. de Melo, M. Hor-Meyll, A. Salles, S. P. Walborn, P. H. Souto Ribeiro, and L. Davidovich, "Environment-induced sudden death of entanglement," Science **316**, 579–582 (2007).
41. J.-C. Lee, Y.-C. Jeong, Y.-S. Kim, and Y.-H. Kim, "Experimental demonstration of decoherence suppression via quantum measurement reversal," Opt. Express **19**, 16309–16316 (2011).
42. Y.-S. Kim, J.-C. Lee, O. Kwon, and Y.-H. Kim, "Protecting entanglement from decoherence using weak measurement and quantum measurement reversal," Nat. Phys. **8**, 117–120 (2012).
43. H.-T. Lim, J.-C. Lee, K.-H. Hong, and Y.-H. Kim, "Avoiding entanglement sudden death using single-qubit quantum measurement reversal," Opt. Express **22**, 19055–19068 (2014).
44. H.-T. Lim, J.-C. Lee, K.-H. Hong, and Y.-H. Kim, "Observation of decoherence-induced exchange symmetry breaking in an entangled state," Phys. Rev. A **90**, 052328 (2014).
45. I. Marcikic, H. de Riedmatten, W. Tittel, H. Zbinden, M. Legré, and N. Gisin, "Distribution of time-bin entangled qubits over 50 km of optical fiber," Phys. Rev. Lett. **93**, 180502 (2004).
46. O. Kwon, K. K. Park, Y.-S. Ra, Y.-S. Kim, and Y.-H. Kim, "Time-bin entangled photon pairs from spontaneous parametric down-conversion pumped by a cw multi-mode diode laser," Opt. Express **21**, 25492–25500 (2013).
47. W. K. Wootters, "Entanglement of formation of an arbitrary state of two qubits," Phys. Rev. Lett. **80**, 2245–2248 (1998).
48. Y.-H. Kim, "Measurement of one-photon and two-photon wave packets in spontaneous parametric downconversion," J. Opt. Soc. Am. B **20**, 1959–1966 (2003).